

 Open access • Journal Article • DOI:10.1063/1.1145562

Trace gas detection with cavity ring down spectroscopy — [Source link](#)





Rienk T. Jongma, Maarten G. H. Boogaarts, Iwan Holleman, Gerard Meijer

Published on: 01 Apr 1995 - Review of Scientific Instruments (American Institute of Physics)

Topics: Cavity ring-down spectroscopy, Absorption spectroscopy, Trace gas, Spectroscopy and Detection limit

Related papers:

- [Cavity ring-down optical spectrometer for absorption measurements using pulsed laser sources](#)
- [Cavity ring-down spectroscopy for quantitative absorption measurements](#)
- [Cavity ring-down spectroscopy: Experimental schemes and applications](#)
- [Coherent cavity ring down spectroscopy](#)
- [CW cavity ring down spectroscopy](#)

Share this paper:    

View more about this paper here: <https://typeset.io/papers/trace-gas-detection-with-cavity-ring-down-spectroscopy-vpyqvjd27t>



PDF hosted at the Radboud Repository of the Radboud University Nijmegen

The following full text is a publisher's version.

For additional information about this publication click this link.

<http://hdl.handle.net/2066/99014>

Please be advised that this information was generated on 2022-05-29 and may be subject to change.

Trace gas detection with cavity ring down spectroscopy

Rienk T. Jongma, Maarten G. H. Boogaarts, Iwan Holleman, and Gerard Meijer

Citation: *Rev. Sci. Instrum.* **66**, 2821 (1995); doi: 10.1063/1.1145562

View online: <http://dx.doi.org/10.1063/1.1145562>

View Table of Contents: <http://rsi.aip.org/resource/1/RSINAK/v66/i4>

Published by the [American Institute of Physics](#).

Related Articles

Depth-resolved cathodoluminescence spectroscopy of silicon supersaturated with sulfur
Appl. Phys. Lett. **102**, 031909 (2013)

Effect of plasma N₂ and thermal NH₃ nitridation in HfO₂ for ultrathin equivalent oxide thickness
J. Appl. Phys. **113**, 044103 (2013)

Atomic-scale characterization of germanium isotopic multilayers by atom probe tomography
J. Appl. Phys. **113**, 026101 (2013)

Monitoring metal contamination of silicon by multiwavelength room temperature photoluminescence spectroscopy
AIP Advances **2**, 042164 (2012)

Annealing studies of heteroepitaxial InSbN on GaAs grown by molecular beam epitaxy for long-wavelength infrared detectors
J. Appl. Phys. **112**, 083107 (2012)

Additional information on Rev. Sci. Instrum.


Journal Homepage: <http://rsi.aip.org>

Journal Information: http://rsi.aip.org/about/about_the_journal

Top downloads: http://rsi.aip.org/features/most_downloaded

Information for Authors: <http://rsi.aip.org/authors>

ADVERTISEMENT



JANIS

Does your research require low temperatures? Contact Janis today.
Our engineers will assist you in choosing the best system for your application.

10 mK to 800 K	LHe/LN ₂ Cryostats
Cryocoolers	Magnet Systems
Dilution Refrigerator Systems	
Micro-manipulated Probe Stations	

sales@janis.com www.janis.com
Click to view our product web page.

Trace gas detection with cavity ring down spectroscopy

Rienk T. Jongma, Maarten G. H. Boogaarts, Iwan Holleman, and Gerard Meijer^{a)}

Department of Molecular and Laser Physics, University of Nijmegen, Toernooiveld, 6525 ED, Nijmegen, The Netherlands

(Received 9 January 1995; accepted for publication 12 January 1995)

Trace gas detection of small molecules has been performed with cavity ring down (CRD) absorption spectroscopy in the near UV part of the spectrum. The absolute concentration of the OH radical present in trace amounts in heated plain air due to thermal dissociation of H₂O has been calibrated as a function of temperature in the 720–1125 °C range. Detection of NH₃ at the 10 ppb level is demonstrated in calibrated NH₃/air flows. Detection of the background Hg concentration in plain air is performed with a current detection limit below 1 ppt. The effect of the laser linewidth in relation to the width of the absorption line is discussed in detail. Basic considerations regarding the use of CRD for trace gas detection are given and it is concluded that CRD spectroscopy holds great promise for sensitive [(sub)-ppb] and fast (kHz) detection of many small molecules. © 1995 American Institute of Physics.

I. INTRODUCTION

Over the last years optical spectroscopic techniques have gained considerable interest for trace gas detection.¹ Among the unique features relevant for air monitoring that these techniques can offer are the high sensitivity due to the species and internal-state selectivity, the nonintrusive and the quantitative character, the fast time response as well as the possibility of remote sensing. High sensitivity is particularly obtained when background-free spectroscopic techniques like photoacoustic spectroscopy, photothermal deflection, or laser-induced fluorescence are used. The quantitative character of spectroscopic techniques is fully employed when the wavelength-dependent direct absorption of a sample is monitored, as in differential optical absorption spectroscopy (DOAS) and in differential absorption lidar (DIAL). With the use of long absorption path lengths (up to tens of km), a high sensitivity can be achieved with these latter techniques as well.

In 1988 O'Keefe and Deacon² introduced cavity ring down (CRD) spectroscopy as a sensitive technique to perform direct absorption measurements using pulsed light sources. The CRD technique is based on a measurement of the rate of absorption rather than the magnitude of absorption of a light pulse confined in an optical cavity with a high-*Q* factor. The method has the aforementioned advantages of direct absorption spectroscopic techniques but sensitivity problems due to light source intensity fluctuations are circumvented and a stable optical cavity design allows for highly effective multipassing. O'Keefe and Deacon already showed in their first experiments that the sensitivity of the method in the visible region of the spectrum is superior to the sensitivity of conventional absorption spectroscopy. Since then O'Keefe *et al.*³ demonstrated that this technique can be used to perform sensitive absorption spectroscopy in a molecular jet expansion. Romanini and Lehmann⁴ have used CRD for a spectroscopic study of the stretching overtones in HCN. In these experiments mirrors with a reflectivity

$R \geq 0.9999$ were used and a noise-equivalent absorption coefficient in the 10^{-10} cm^{-1} range was reported. Yu and Lin⁵ have shown that CRD can be used for quantitative kinetics measurements as well. We have recently shown that CRD spectroscopy can be performed with a high spectral resolution and a good sensitivity even in relatively short cavities and have applied the technique for the first time in the UV part of the spectrum,⁶ even down to 200 nm.⁷ Around 250 nm, where no mirrors with a reflectivity better than $R = 0.997$ are available yet, absorption down to 10^{-7} cm^{-1} is still readily detected.⁸

In this paper we report on the use of CRD spectroscopy in the near UV for trace gas detection. It is the near UV part of the spectrum that is particularly well suited for trace gas detection as many small molecules have strong, well-characterized absorption bands in this region. The CRD technique has been applied to calibrate the absolute concentration of the OH radical present in trace amounts in heated plain air via probing of OH on the $A^2\Sigma^+(v'=0) \leftarrow X^2\Pi(v''=0)$ transition around 309 nm. It was shown recently⁹ that OH formed via thermal dissociation of H₂O in the 1200–1600 °C range is present in detectable quantities, and can therefore be used as a calibration standard for other studies. In this study⁹ the OH radical was detected via laser-induced fluorescence (LIF) and the relative concentration of OH at different temperatures was measured. From LIF measurements it is difficult, however, to extract the absolute OH concentration as a function of temperature which was consequently calculated rather than experimentally determined. In our CRD experiments we have been able to determine the absolute concentration of OH as a function of temperature and to do so at relatively low temperatures in the 720–1125 °C range. The CRD technique has also been applied for detection of NH₃ in calibrated NH₃/air flows via absorption detection on the $\tilde{A} \leftarrow \tilde{X}(3\nu_2 \leftarrow 0)$ transition of NH₃ around 205 nm. Atomic Hg vapor, present in ppt concentrations in air,¹⁰ is detected via CRD on the strong transition around 253.7 nm with sub-ppt sensitivity. An in depth discussion of a kind of “saturation” effect that occurs when the bandwidth of the light source can no longer be neglected relative to the width

^{a)}E-mail: gerardm@sci.kun.nl

of the molecular absorption is presented. Basic considerations regarding the use of CRD for trace gas detection are given and, based on the presented measurements, it is concluded that CRD spectroscopy holds great promise for sensitive [(sub)-ppb] and fast (kHz) detection of many small molecules.

II. CAVITY RING DOWN SPECTROSCOPY

In a typical CRD experiment, a light pulse with a spectral intensity distribution $I(\nu)$ and a duration T which is short with respect to the "cavity ring down time" $\tau(\nu)$ (*vide infra*) is coupled into a stable optical cavity with highly reflecting mirrors.⁶ The fraction of the light pulse that is successfully coupled into the cavity bounces back and forth many times between the mirrors and the light intensity inside the cavity is an exponentially decaying function of time. The time-dependent light intensity inside the cavity, $I_{\text{CRD}}(t)$, can be most conveniently monitored via the small fraction of light that is transmitted through one of the mirrors.

If a monochromatic light pulse at frequency ν is coupled into an otherwise empty cavity, the ring down transient $I_{\text{CRD}}(t)$ is a single exponentially decaying function of time with a $1/e$ cavity ring down time $\tau(\nu)$ which is solely determined by the reflectivity $R(\nu)$ of the mirrors and the optical path length d between the mirrors. The presence of absorbing species in the ring down cavity can now be deduced from a resulting decrease in the cavity ring down time. It follows, therefore, that in the more general case $I_{\text{CRD}}(t)$ is proportional to

$$I_{\text{CRD}}(t) \propto \int_0^\infty I(\nu) e^{-t/\tau(\nu)} d\nu, \quad (1)$$

where $\tau(\nu)$ is given by

$$\tau(\nu) = \frac{d}{c[\ln(R(\nu)) + \sum_i \sigma_i(\nu) \int_0^d N_i(x) dx]} \quad (2)$$

and the sum is over all light scattering and absorbing species with frequency-dependent cross sections $\sigma_i(\nu)$ and a line-integrated number density $\int_0^d N_i(x) dx$. When considering narrow frequency intervals the frequency dependence of Rayleigh [$\sigma_{\text{Rai}}(\nu)$] and Mie [$\sigma_{\text{Mie}}(\nu)$] scattering as well as of the mirror reflectivity can be neglected, and an effective loss factor $|\ln(R_{\text{eff}})|$ that can also contain broadband absorption is taken. The product of the frequency-dependent absorption cross section $\sigma_i(\nu)$ with the number density $N_i(x)$ is commonly expressed as the absorption coefficient $\kappa_i(\nu, x)$ and the line-integrated absorption coefficient can be extracted from a measurement of the cavity ring down transient. In many cases the line-integrated number density will be constant in time, but even if there is any time dependence of $\int_0^d N_i(x) dx$ this can be extracted from the ring down transient and dynamical processes can be studied this way.⁵ The temporal profile of the CRD transient is obviously independent of the amplitude of the light circulating inside the cavity and is solely a property of the cavity and the absorbing species.

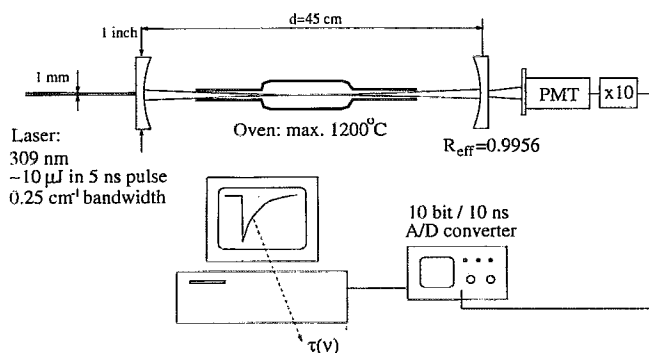


FIG. 1. Schematic overview of the experimental setup used for calibration of the OH concentration in heated plain air. CRD absorption measurements are performed through the oven in the 309 nm region where the OH absorption is strongest.

III. EXPERIMENTAL SETUP

A schematic overview of the experimental setup used for the detection of trace amounts of OH in heated air with CRD is given in Fig. 1. A stable optical cavity is formed by placing two identical 25-mm-diam plano-concave mirrors with a radius of curvature of -25 cm at 45 cm distance. The mirrors are coated for optimum reflectivity at 308 nm ($R_{\text{eff}} = 0.9956$ at 309 nm). A quartz tube of 34 cm total length with open ends located in a temperature stabilized oven is centered in the ring down cavity. The end parts of the quartz tube have 7 -mm-diam openings and have a length/diameter ratio of 11 , thereby resembling the oven as used by Grinstead *et al.*⁹ The middle 15 cm of the quartz tube is (more or less) homogeneously heated to temperatures in the 750 – 1200 °C range, leading to air temperatures inside the quartz tube between 720 and 1125 °C.

The OH radicals can be most efficiently detected on the $A^2\Sigma^+(v'=0) \leftarrow X^2\Pi(v''=0)$ electronic transition around 309 nm. The required light pulses at this wavelength are produced by frequency doubling the output of a Nd:YAG laser pumped pulsed dye laser system (Spectra Physics GCR-150, PDL-3) in a KDP crystal. Only a few nJ/pulse of the 309 nm radiation (0.25 cm⁻¹ bandwidth) is coupled into the cavity through one of the mirrors. Mode matching of the laser beam with the ring down cavity is omitted as to set up a near continuum of modes inside the cavity.⁶

The light leaking out of the cavity is detected with a fast photomultiplier (PMT) positioned directly behind the other mirror. The PMT signal is amplified and fed into a digitizing oscilloscope with a 10 -bit vertical resolution and sampling every 10 ns (LeCroy 9430). Typically, some 30 ring down transients all taken at the same laser frequency are added in a 16 -bit memory of the oscilloscope and the sum is subsequently read out by a 486 -PC. To be able to accurately determine the baseline of the cavity ring down transients approximately 100 data points prior to the start of the ring down transient are recorded and averaged. From those data points of the ring down transient that are recorded within a preset time interval from the start of the transient, a time interval which is typically chosen as three $1/e$ decay times of the empty cavity, this averaged baseline value is subtracted.

Subsequently, the natural logarithm of the data is taken and fit to a straight line using a least-squares weighted fitting algorithm.¹¹ It is the slope of this fitted line which is recorded as a function of the laser frequency. It should be explicitly noted, and it is evident from Eqs. (1) and (2), that only in the case of a monochromatic light pulse and only if the line-integrated number density $\int_0^d N_i(x)dx$ is time independent, the ring down transient can be fit exactly to a single exponentially decaying curve as assumed in this data reduction algorithm.

To accurately determine the absolute concentration of OH in heated plain air as a function of temperature parts of the electronic $A^2\Sigma^+(v'=0) \leftarrow X^2\Pi(v''=0)$ absorption spectrum of OH are measured with CRD for each temperature. These parts are chosen as to contain a sufficiently large number of well-resolved rotational lines that have a high temperature sensitivity in their relative intensity distribution.

The NH_3 absorption experiments are performed in a similar experimental setup but now with a closed-off ring down cavity through which calibrated NH_3 /air mixtures are flowing. The NH_3 concentration in the flowing air mixture is monitored by a chemiluminescence detector after exiting the ring down cavity. This detector actually detects NO_x formed via oxidation of NH_3 with a 100% efficiency in an oven. The ring down cavity is made of Teflon to avoid the sticking of NH_3 to the walls of the cavity as much as possible. The cavity length is again 45 cm and mirrors coated for optimum reflectivity at 206 nm ($R_{\text{eff}}=0.985$) are used. In this wavelength region the NH_3 molecules can be detected via absorption on the strong $\tilde{A} \leftarrow \tilde{X}$ electronic transition. Tunable radiation in the 204–207 nm region with a 0.3 cm^{-1} bandwidth is obtained by frequency tripling the fundamental output of the dye laser in a combination of a KDP and a BBO crystal. To determine the absorption detection limit for NH_3 with CRD in our ring down cavity measurements have been performed at two fixed laser frequencies only. The ring down time has been recorded both on top of a strong NH_3 resonance and in between NH_3 resonances as a function of the NH_3 concentration in the calibrated flow.

The Hg absorption measurements are performed in an open cavity of 45 cm length, consisting of two mirrors coated for optimum reflectivity at 248 nm ($R_{\text{eff}}=0.996$). Laser radiation in the 250–255 nm range is produced by pumping a Coumarin 500 dye laser with the third harmonic of the Nd:YAG laser at 355 nm. The output of the dye laser is frequency doubled in a BBO crystal providing laser radiation with a bandwidth of 0.1 cm^{-1} .

IV. RESULTS AND DISCUSSION

A. Detection of OH in heated air

To determine the absolute concentration of OH present in heated plain air the cavity ring down time is recorded as a function of laser frequency at various oven temperatures. For oven temperatures between 750 and 950 °C three regions of the OH $A \leftarrow X$ (0,0) band are selected, from 32 279 to 32 300 cm^{-1} , from 32 321 to 32 343 cm^{-1} , and from 32 585 to 32 595 cm^{-1} . In these regions of the spectrum numerous lines with large absorption cross sections starting from rota-

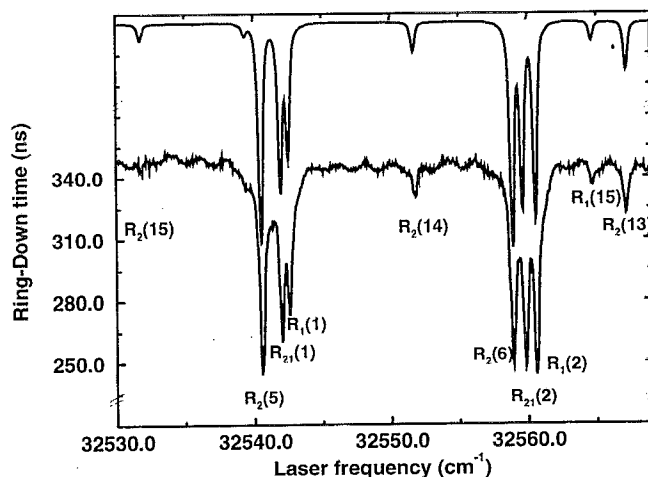


FIG. 2. Lower trace: CRD spectrum of OH measured at an oven temperature of 1000 °C. Assignment of the strongest OH $A^2\Sigma^+(v'=0) \leftarrow X^2\Pi(v''=0)$ absorption lines is made in the figure. Upper trace: Simulated CRD spectrum, obtained by calculating the ring down transient for each laser frequency and fitting a single exponentially decaying curve with a ring down time τ to this transient. The spectral intensity distribution of the radiation source as well as the Doppler broadened shape of the absorption line are taken into account in this simulation.

tional energy levels with a vastly different Boltzmann population are present. This assures a good detection efficiency in combination with a high temperature sensitivity. For oven temperatures in the 1000–1200 °C range the OH absorption in these regions of the spectrum starts to show saturation effects and the 32 530–32 570 cm^{-1} region which contains weaker lines is selected for concentration and temperature calibration.

In the lower trace of Fig. 2 the CRD spectrum of heated air as measured at an oven temperature of 1000 °C is shown. The actual measured ring down time (in ns) is plotted as a function of laser frequency. All observed lines in the spectrum are readily identified using the known OH transition frequencies¹² and the strongest lines are indicated in the figure. The top trace in this figure shows the simulated CRD spectrum of OH on the same scale but shifted upward by a fixed amount. This spectrum has been obtained by calculating the ring down transient for each laser frequency and then applying the same data-reduction routine as used in the actual measurements. To calculate the ring down transient at a given laser frequency Eqs. (1) and (2) are used. A Lorentzian laser profile $I(\nu)$ with a full width at half maximum of 0.25 cm^{-1} is taken as this matches best to the experimental observations. In the calculations we have further used an effective mirror reflectivity R_{eff} for the entire spectrum which is deduced from the averaged observed baseline ring down time. It is assumed in the calculation that the relative number density for the various rotational levels that are probed in the spectrum is determined by a Boltzmann distribution with a single rotational temperature T_{rot} . The known OH transition frequencies and absolute absorption cross sections^{12,13} corrected for the variation of transition dipole moment with rotational quantum number¹⁴ are taken. All our calculations are scaled relative to the $P_1(1)$ transition, for which an oscillator strength of 6.02×10^{-4} is taken.¹³ The shape of the absorp-

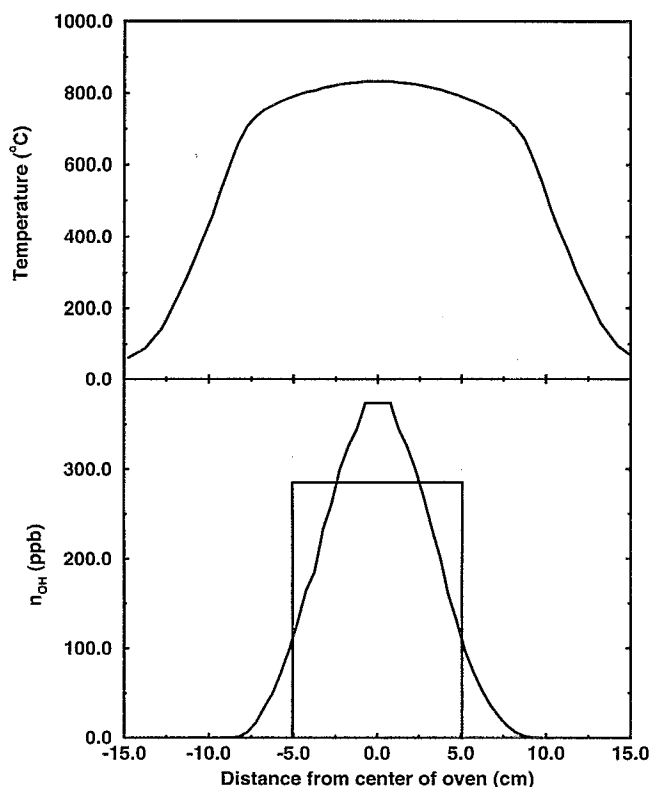


FIG. 3. Upper figure: Temperature profile of the oven at an oven temperature of 850 °C. Lower figure: The peaked distribution function shows the OH concentration as calculated from the measured temperature profile using the calculated dependence of the OH mole fraction on temperature (Ref. 9). The block-distribution function shows the OH concentration as assumed in the simulation. The latter distribution yields the same averaged temperature and the same line-integrated OH number density as the actual OH distribution function.

tion lines is taken to be Gaussian with a width determined by the Doppler broadening at the temperature T_{rot} . The total number density of OH summed over all internal rovibrational levels follows from matching the calculated ring down time on all absorption lines to the observed absolute values, assuming homogeneous OH absorption over a 10 cm path length, as will be explained below.

In the upper part of Fig. 3 the temperature of the air inside the oven as measured with a free-hanging thermocouple on the axis of the oven is given for an oven temperature of 850 °C. It is seen that in the middle 15 cm of the oven the temperature is approximately constant and is slightly lower than the oven temperature as measured with a thermocouple on the oven walls. As the mole fraction of OH is strongly dependent on the temperature it varies strongly as a function of the position in the oven, even over the “flat” temperature range. If we assume that the calculated temperature dependence of the mole fraction of OH as given by Grinstead *et al.*⁹ can be extrapolated to the lower temperatures used here, an assumption that is corroborated by the outcome of our experiments, a sharply peaked OH distribution in the oven as given in the lower part of Fig. 3 is obtained. The advantage of this sharply peaked OH distribution is that it allows to take a single averaged temperature to describe the internal energy distribution and the absorption

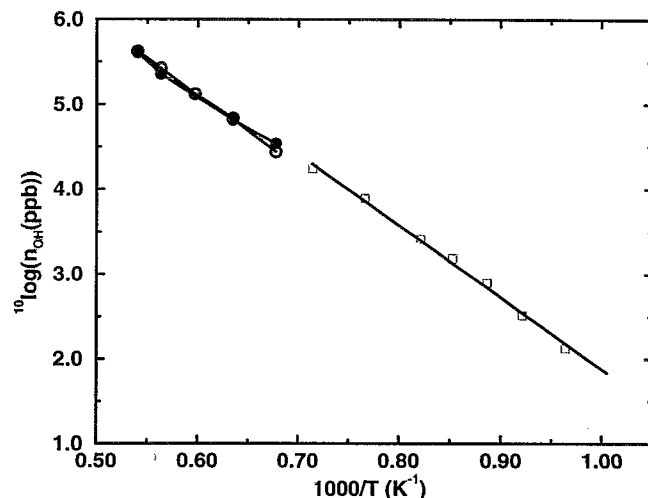


FIG. 4. Logarithmic plot of the total OH mole fraction in parts per billion (ppb) as a function of $1/T$. The open squares are the results obtained by the CRD direct absorption measurements. The best straight line fit through the data is also shown in the figure. The open circles represent the calculated values of Grinstead *et al.* (Ref. 9), whereas the filled circles show their experimental values obtained by scaling the values extracted from their LIF measurements to their calculations.

linewidth of the OH molecules as these are not as critically dependent on the temperature as the absolute OH number density. This averaged temperature T_{avg} is obtained by averaging the actual temperature profile after weighing it with the OH distribution, and amounts to $T_{\text{avg}} = T_{\text{rot}} = 817$ °C when the oven temperature is 850 °C. In the data analysis the actual OH distribution in the oven as discussed above is replaced by a block distribution which yields the same line-integrated OH number density. The length of the block distribution is chosen to yield the same averaged temperature and is thereby uniquely determined. For the temperatures we have used, a homogeneous OH distribution over path length that varies between 10 and 11 cm has been found. It is explicitly noted that the vertical scale of the OH distribution is adjusted afterward to the total number density of OH molecules as deduced from the CRD measurements.

From the various CRD spectra measured at fixed oven temperatures the absolute number density of the OH molecules at the corresponding temperature T_{avg} is determined. Grinstead *et al.* found that the OH molecules, present in heated plain air, are formed via thermal dissociation of H_2O . In accordance with this, we scaled the OH number densities, we found linearly with the air humidity to an averaged air humidity of 55% (the air humidity varied between 44% and 60% in the course of the measurements) and have plotted the thus obtained OH mole fraction as a function of $1/T$ in an Arrhenius plot in Fig. 4. In this figure the open squares are our experimental data points. In the high-temperature region the theoretical and experimental data points of Grinstead *et al.* are indicated by open and filled circles, respectively. Also shown in the figure is the best straight line fit to our experimental data points. The OH mole fraction measured at the lowest temperature has been omitted from this fit as it deviates strongly from the fit for as yet unknown reasons.

The best fit to our data yields an OH mole fraction as a function of temperature in the 765–1125 °C range at a relative air humidity of 55% given by

$$^{10}\log[n_{\text{OH}}(T)(ppb)] = (10.41 \pm 0.22) - \frac{(8530 \pm 250)}{T(\text{K})}. \quad (3)$$

The temperature dependence of the OH mole fraction is within the error limits the same as the value that follows from the calculations by Grinstead *et al.* This suggests Eq. (3) holds over the whole 765–1600 °C temperature range, although the prefactor can not be extracted directly from their data without knowledge of the exact value of the air humidity that is taken.

B. Linewidth effects

It is evident from the equations given in Sec. II that the cavity ring down transient is only a single exponentially decaying curve if the width of the radiation that is coupled into the cavity is much smaller than the width of the absorption features. For the experiments discussed above we used a laser with a Lorentzian spectral profile with a full width at half maximum of $\Delta\nu_{\text{las}} = 0.25 \text{ cm}^{-1}$ whereas the OH absorption lines are Doppler broadened to approximately $\Delta\nu_{\text{mol}} = 0.2 \text{ cm}^{-1}$ and therefore a multiexponential behavior is expected. To illustrate this multiexponential behavior, both measured and simulated ring down transients with the laser on top of the $P_1(4)$ transition of OH at $32\,289.12 \text{ cm}^{-1}$ are shown in Fig. 5. The measurement is performed at an oven temperature of 950 °C where the absorption on the $P_1(4)$ line is such that $\sim 0.35\%$ of the laser radiation is absorbed in the first passage through the oven. In the inset of both the experimental and simulated ring down transients the logarithmic plot of the data is shown, together with the straight line fit as determined by the fitting algorithm we used. The use of a weighted least-squares fitting algorithm implies that the obtained value for the ring down time is predominantly determined by the first part of the ring down transient. Especially for the later part of the ring down transient, both the experimental and the simulated curves show a clear but identical deviation from a single-exponential behavior. As the data reduction algorithm in our CRD experiment is based on the assumption of single exponentially decaying curves, this deviation will lead to an underestimate of the absorption and cause a kind of “saturation” effect in the CRD absorption spectra.

In Fig. 6 the calculated effect of the laser bandwidth on the absorption strength as measured with CRD spectroscopy is shown as a function of the actual absorption strength. The absorption strength determined with CRD is given by $1/(c\tau)$, where τ is obtained assuming a single exponentially decaying curve as described in Sec. III. In the calculation, a Gaussian frequency profile with a full width at half maximum of 0.2 cm^{-1} is assumed for the absorption line whereas a Lorentzian spectral profile with a varying width, indicated in the figure, is taken for the laser. When the laser is spectrally narrow compared to the absorption line the correct value of the absorption strength follows directly from the CRD experiment as $1/(c\tau)$, once the “offset” due to broadband cav-

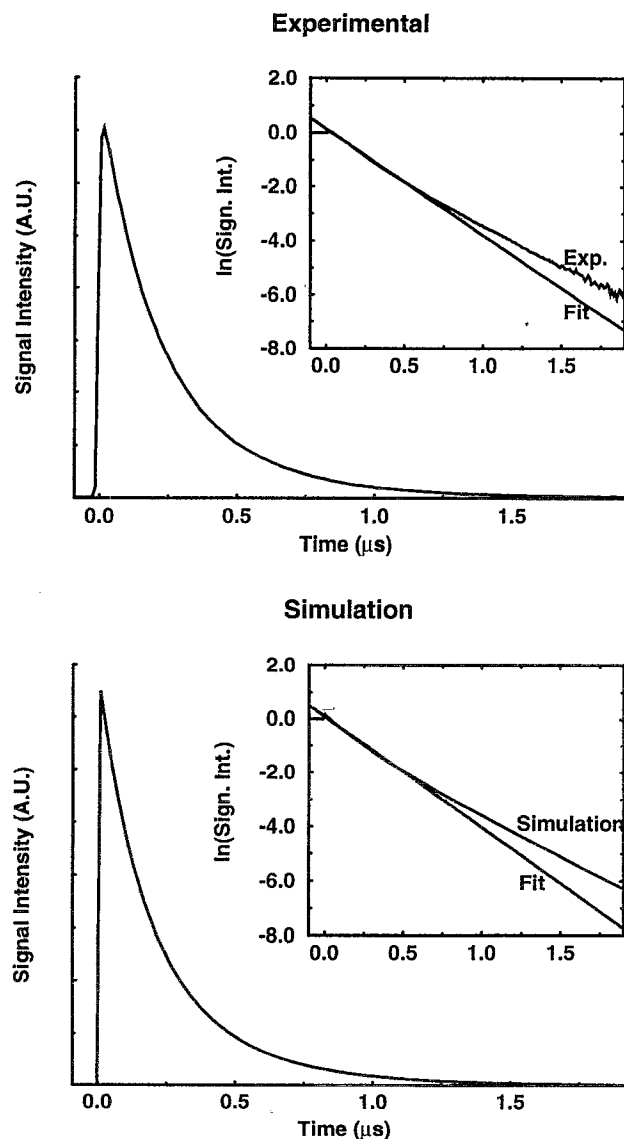


FIG. 5. Upper figure: Experimentally observed ring down transient with the laser on top of the OH ($A \leftarrow X$) $P_1(4)$ transition at $32\,289.12 \text{ cm}^{-1}$. The multiexponential behavior of the ring down transient is evident from the deviation of the logarithm of the data from a best-fitting straight line, as shown in the inset. Lower figure: Simulated ring down transient and logarithmic plot of the data for the same experimental conditions.

ity losses (represented by R_{eff}) is subtracted. This situation is represented in the figure by the line with a slope equal to one for a laser bandwidth of 0.005 cm^{-1} . As can be deduced from the figure, this slope is more generally approximated for a weak absorption by $\Delta\nu_{\text{mol}}/(\Delta\nu_{\text{mol}} + \Delta\nu_{\text{las}})$, identical to the result obtained in conventional direct absorption spectroscopy. It is evident from the figure that, when applied in this way, the CRD detection technique loses its linearity for increasing absorption when the bandwidth of the radiation source can no longer be neglected relative to the width of the absorption features. In addition to this, the inset of Fig. 6 shows that if one considers a very strong absorption, the technique no longer yields a unique absorption strength from a given observed ring down time. This is readily understood if one considers a strong but narrow absorption at the center

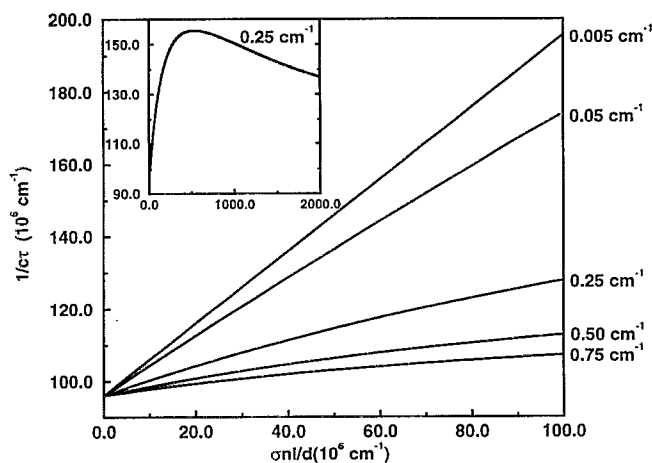


FIG. 6. Calculated effect of the laser bandwidth on the absorption strength as measured with CRD spectroscopy as a function of the actual absorption strength. The vertical offset at zero absorption is caused by radiation losses represented by R_{eff} . In the calculation, a Gaussian frequency profile with a full width at half maximum of 0.2 cm^{-1} is assumed for the absorption line whereas a Lorentzian spectral profile with a varying width, as indicated in the figure, is taken for the laser.

of a relatively broad laser profile; radiation with a frequency at the center of the absorption line will have a short cavity ring down time whereas frequencies in the wings of the laser profile will contribute to the ring down transient over a much longer period of time. With increasing absorption strength the cavity ring down time will first decrease but ultimately it will increase again as radiation at frequencies close to the peak absorption rapidly disappears and the measured cavity ring down time is predominantly determined by frequency components in the wings of the laser profile.

It is important to note that if these linewidth effects are taken into account in the way we described it in the previous section, the CRD technique remains quantitative over a large range of absorption strengths, even if a single exponential decay is fitted to the multiexponential decaying curve. If one would record the full ring down transient as a function of laser frequency the spectral intensity distribution of the radiation source can be canceled out completely and spectra with a resolution limited by the intrinsic width of the molecular absorption can be recorded. In this case the multiexponential behavior of the CRD transients is used to advantage and yields additional information rather than that it complicates the data analysis. Ultimately, this might enable a multiplex cavity ring down spectrometer to be constructed.

C. Trace gas detection limits

From the OH absorption measurements a noise-equivalent absorption detection limit of approximately 6 ppb is found for the lowest oven temperatures we have used. Using the same experimental setup, the absorption detection limit for room-temperature OH will be roughly a factor 10 better due to the combination of a more favorable partition sum (a larger fraction of the OH molecules can be probed via a single transition) and the higher density at lower temperatures. In addition, the entire cavity length can be used for

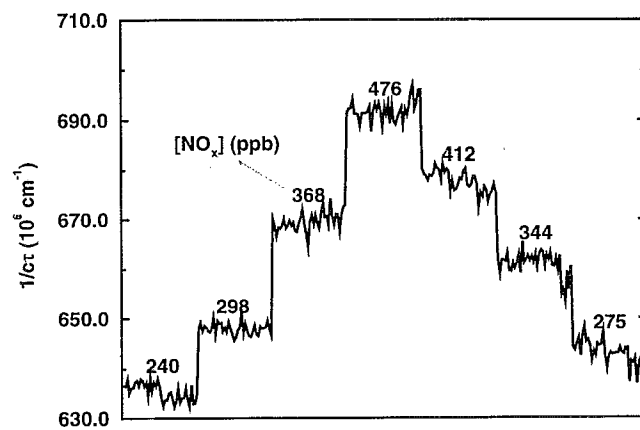


FIG. 7. CRD absorption for calibrated NH_3 /air flows measured via absorption on the $\text{NH}_3 \tilde{A} \leftarrow \tilde{X}(3\nu_2 \leftarrow 0)$ transition at 204.63 nm.

absorption improving the detection limit by another factor 4.5. In the present experimental setup a detection limit of room-temperature OH of better than 0.15 ppb is therefore anticipated. A further improvement of the detection sensitivity is obtained when a narrow-band radiation source is used; it can be read from Fig. 6 that a factor 2.2 can still be gained relative to the present situation.

Detection of trace amounts of NH_3 in calibrated NH_3 /air flows has been demonstrated with CRD around 205 nm. In Fig. 7 the NH_3 absorption as deduced from the CRD transients, given by $1/(c\tau)$, is plotted for several calibrated NH_3 /air flows. Calibration is performed via an NO_x monitor, as described in Sec. III. For this measurement the laser frequency was kept fixed at 204.63 nm, resonant with the $\tilde{A} \leftarrow \tilde{X}(3\nu_2 \leftarrow 0)$ transition.¹⁵ The upper state of this transition is a predissociative state, yielding $\text{NH}_2 + \text{H}$, with a homogeneous linewidth of approximately 80 cm^{-1} . At room temperature, the NH_3 absorption spectrum in the 200–215 nm region consists of a long progression of broad but still well-resolved vibrational transitions. Linewidth effects can be neglected in this situation and single exponentially decaying curves are observed. From the measured data points the absorption coefficient of NH_3 at 204.63 nm is found as $248 \pm 7 \text{ cm}^{-1} \text{ atm}^{-1}$, in good agreement with literature values.¹⁶ It is concluded from these measurements that the noise-equivalent absorption detection limit for NH_3 is around 10 ppb in this setup, although it is likely that part of the apparent noise is actually due to real fluctuations in the NH_3 concentration in the flow, fluctuations that can not be identified as such by the chemi-luminescence detector.

Detection of Hg at the natural occurring background level in plain air is performed via CRD around 253.7 nm. Figure 8 shows the CRD absorption spectrum in the region of interest, where the absorption strength as determined via CRD is given by $1/(c\tau)$. The absorption lines of the forbidden $\text{O}_2 \tilde{A} \leftarrow \tilde{X}(7,0)$ transition ($N''=19$, Q multiplet) are readily identified.¹⁷ The somewhat broader line around $39\,412 \text{ cm}^{-1}$ is due to absorption of Hg. This line consists of pressure broadened overlapping lines of the various stable isotopes of Hg. The effective absorption cross section for this Hg line under atmospheric conditions is determined as

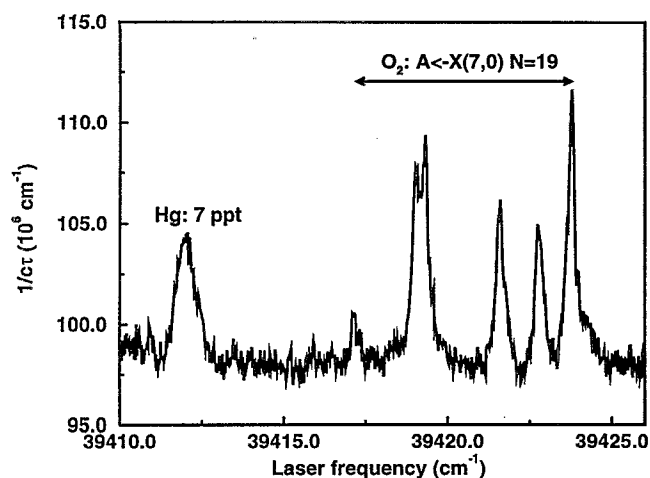


FIG. 8. CRD spectrum of plain air measured in an open cavity. The absorption lines at high frequencies are due to the weak $O_2 A \leftarrow X(7,0)$ band. At 39412 cm^{-1} the absorption of atomic mercury vapor, present at a concentration of 7 ppt, is seen.

$3.3 \times 10^{-14}\text{ cm}^2$.¹⁰ Under the present experimental conditions the laser bandwidth is narrower than the width of the absorption line, and a natural occurring background concentration of Hg in our laboratory of 7 ppt is deduced from these measurements. The noise-equivalent detection limit for Hg is determined from this measurement to be just below 1 ppt.

Like in conventional absorption spectroscopy, differential CRD absorption spectroscopy has to be applied for a quantitative measurement. In the NH_3 experiments we made separate measurements around 206.55 nm , where the NH_3 absorption is minimum, to subtract the background radiation losses of the cavity. To perform differential CRD absorption spectroscopy more elegantly, two light pulses with a slightly different wavelength can be coupled into the cavity shortly after each other and be separated in time, or they can be coupled into the cavity simultaneously and be separated via wavelength or polarization selection.

For many other small molecules detection limits in the (sub)-ppb range will be obtainable with CRD in the near UV part of the spectrum. Most molecules have their strongest transitions in this region and for small molecules the spectra are still structured enough that they are truly species selective. From a comparison with detection limits in differential optical absorption spectroscopy (DOAS),¹ it is concluded that detection of for instance SO_2 , CS_2 , NO , NO_2 , and O_3 can be performed at the ppb level with CRD in the near UV with presently available optics in relatively short cavities.

Increase of the cavity length is an obvious way to improve on the detection sensitivity. Not only does the absorption length increase linearly with the cavity length but in addition the absolute accuracy with which the cavity ring down time can be determined will get better as the ring down transient is recorded over a longer time interval. It should be noted that the maximum obtainable cavity ring down time is limited by the Rayleigh and Mie scattering and is independent of the cavity length in that case, as can be seen from Eq. (2). When increasing the cavity length above $|\ln(R(\nu))|/([\sigma_{\text{Rai}}(\nu) + \sigma_{\text{Mie}}(\nu)]N_{\text{tot}})$, where N_{tot} is the total

number density of scattering species, Rayleigh and Mie scattering will be more important loss factors than the reflection losses on the mirrors. For the OH detection in air around 309 nm , this implies that the maximum cavity ring down time that can be obtained is on the order of $10\text{ }\mu\text{s}$. With our present highly reflecting 309 nm mirrors with reflection coefficients around $R=0.996$, an increase of the cavity length above 10 m will not significantly improve the detection sensitivity.

In the experiments described here a laser system at a 10 Hz repetition frequency is used and the ring down transients are summed over 30 laser shots, yielding a data point every 3 s. The actual measurement time is only $30\text{ }\mu\text{s}$, however, and it should be possible therefore to make absorption measurements at high repetition rates, probably limited by the data collection rate.

Trace gas detection of small molecules has been demonstrated with cavity ring down (CRD) absorption spectroscopy in the near UV part of the spectrum. The absolute concentration of the OH radical present in trace amounts in heated plain air due to thermal dissociation of H_2O has been calibrated as a function of temperature at a relative air humidity of 55%. The noise-equivalent detection limit for room-temperature OH in our present experimental setup is around 0.15 ppb and a detection limit of a few ppt should be obtainable with the suggested improvements. Detection of NH_3 at the 10 ppb level is demonstrated in calibrated NH_3 /air flows and a detection sensitivity below 1 ppt has been obtained for the detection of atomic mercury vapor. A discussion of the kind of "saturation" effects that can occur when the bandwidth of the light source can no longer be neglected relative to the width of the molecular absorption is presented. Basic considerations regarding the use of CRD for trace gas detection are given and, based on the measurements presented here, it is concluded that CRD spectroscopy holds great promise for sensitive [(sub)-ppb] and fast (kHz) detection of many small molecules.

ACKNOWLEDGMENTS

We acknowledge the help of Jules Spaanjaars, Hans Naus, and Erik Vrijenhoek in the OH and Hg measurements and the collaboration with Jos Hogenkamp, Marcel Mennen, and Ton van der Meulen ("Laboratorium voor Lucht Onderzoek," RIVM, Bilthoven, The Netherlands) in the NH_3 measurements. This work is part of the research program of the "Stichting voor Fundamenteel Onderzoek der Materie (FOM)," which is financially supported by the "Nederlandse Organisatie voor Wetenschappelijk Onderzoek (NWO)."

¹ *Air Monitoring by Spectroscopic Techniques*, edited by M. W. Sigrist (Wiley, New York, 1994).

² A. O'Keefe and D. A. G. Deacon, *Rev. Sci. Instrum.* **59**, 2544 (1988).

³ A. O'Keefe, J. J. Scherer, A. L. Cooksy, R. Sheeks, J. Heath, and R. J. Saykally, *Chem. Phys. Lett.* **172**, 214 (1990).

⁴ D. Romanini and K. K. Lehmann, *J. Chem. Phys.* **99**, 6287 (1993).

⁵ T. Yu and M. C. Lin, *J. Am. Chem. Soc.* **115**, 4371 (1993).

⁶ G. Meijer, M. G. H. Boogaarts, R. T. Jongma, D. H. Parker, and A. M. Wodtke, *Chem. Phys. Lett.* **217**, 112 (1994).

⁷ R. T. Jongma, M. G. H. Boogaarts, and G. Meijer, *J. Mol. Spectrosc.* **165**, 303 (1994).

- ⁸D. L. Huestis, R. A. Copeland, K. Knutsen, T. G. Slanger, R. T. Jongma, M. G. H. Boogaarts, and G. Meijer, *Can. J. Phys.* **72**, 1109 (1994).
- ⁹J. H. Grinstead, G. Laufer, R. H. Krauss, and J. C. McDaniel, *Appl. Opt.* **33**, 1115 (1994).
- ¹⁰H. Edner, G. W. Faris, A. Sunesson, and S. Svanberg, *Appl. Opt.* **28**, 921 (1989).
- ¹¹W. H. Press, B. F. Flannery, S. A. Teukolsky, and W. T. Vetterling, *Numerical Recipes in C: The Art of Scientific Computing* (Cambridge University, Cambridge, 1988).
- ¹²G. H. Dieke and H. M. Crosswhite, *J. Quant. Spectrosc. Radiat. Transfer.* **2**, 97 (1962).
- ¹³T. J. McGee and T. J. McIlrath, *J. Quant. Spectrosc. Radiat. Transfer.* **32**, 179 (1984).
- ¹⁴D. R. Yarkony, *J. Chem. Phys.* **97**, 1838 (1992).
- ¹⁵V. Vaida, M. I. McCarthy, P. C. Engelking, P. Rosmus, H. J. Werner, and P. Botchwina, *J. Chem. Phys.* **86**, 6669 (1987).
- ¹⁶K. Watanabe, *J. Chem. Phys.* **22**, 1564 (1954).
- ¹⁷P. M. Borrell, P. Borrell, and D. A. Ramsay, *Can. J. Phys.* **64**, 721 (1986).